JOURNAL OF AIRCRAFT
Vol. 42, No. 1, January–February 2005

Characteristics of Y-Shaped Rectangular Diffusing Duct at Different Inflow Conditions

Titiksh Patel,* S. N. Singh,† and V. Seshadri‡
Indian Institute of Technology, Delhi, New Delhi 110 016, India

Y-Shaped diffusing intake ducts are extensively used for engines in fighter aircrafts. These ducts normally operate under steady and symmetric conditions but, during some maneuvers, the inflow becomes asymmetric. An attempt has been made to analyze the flow characteristics within the Y-shaped rectangular diffusing duct having a turn angle of 22.5/22.5 deg and an overall area ratio of 2.0 with a circular outlet. The inlet of this duct is through two rectangular openings with an aspect ratio of 2.0. Detailed analyses are carried out using the computational fluid dynamics code FLUENT for skewed axial velocity distribution in one limb and uniform flow in the other limb at average inlet velocities of 30, 60, and 90 m/s. The results show that static pressure recovery reduces with increases in skewness, and strong secondary flows are observed throughout the length of the diffuser with a highly complex flow pattern at the merging plane. The performance characteristics of the Y-shaped duct with uniform flow at the inlet of the two limbs is found to be independent of Reynolds number over the range analyzed. Longitudinal velocity contours show the deflection of the flow toward the outer wall all along the length of the diffuser for all inflow conditions.

Nomenclature

C_L	=	coefficient of total pressure loss
C_p	=	coefficient of static pressure recovery
$C_{1\varepsilon}, C_{2\varepsilon}, C\mu, \sigma_k, \sigma_\varepsilon$	=	constants of the turbulence model
G_k	=	generation term (kinetic energy)
k	=	turbulent kinetic energy
R_c	=	radius of curvature
U_{avi}	=	average inlet velocity
$\Delta\beta$	=	angle of turn
ε	=	turbulence dissipation rate

Introduction

ALMOST all modern combat aircraft use fuselage-mounted intake ducts with a bifurcated Y configuration. These intake ducts have to meet the varying flow demands of the engines because these aircraft have to perform highly complicated maneuvers. Present-day engines have a comparatively fewer number of stages and high-pressure ratio per stage and, hence, are very sensitive to flow changes. This dependence requires sustained efforts by the designers to ensure engine-intake compatibility along with optimum integration of the intake with the fuselage. The aerodynamics within these intakes has traditionally been analyzed by resorting to controlled experiments because of the complex nature of flow. Martin and Holzhauser[1] presented a very simplistic theory using an energy equation for analysis of flow through a twin air intake in terms of static pressure and ram pressure as a function of velocity ratio. They found that the flow instability and flow reversal encountered at low velocity ratios is dependent on static pressure recovery rather than ram pressure. Simon[2] evaluated the performance of various types of side inlets mounted on a fuselage at a Mach number of 2.0. He observed that the inlet performance was independent of the operating conditions for all configurations tested. He also found that the rectangular inlet with either 6- or 12-deg external compression ramps exhibited a stable operation range. Obery and Stitt[3] extended the work of Simon[2] to Mach numbers of 1.5 and 1.7. Pai[4] discussed the concepts for aerodynamic testing of air intake with twin design objectives of intake–airframe integration and engine-intake compatibility. Sudhakar and Ananthkrishnan[5] have also proposed a simple flow model for a Y-shaped duct that predicts the boundary for stable symmetric operation marked by a bifurcation, which is present only for maximum pressure recovery. Jolly et al.[6] discussed the design and development of a bifurcated Y-shaped duct used in modern combat aircraft as an intake duct. Recently Bharani et al.[7,8] analyzed the performance of divided intake ducts with a view to understanding the effect of angle of turn, area ratio, and inlet Reynolds number on the performance of the duct. Besides these few studies on Y-shaped ducts, not much information is available in the open literature on these ducts, which is possibly due to the confidential nature of the work. However, several studies pertaining to single S-shaped diffusing ducts are available. Guo and Seddon[9–11] attempted to understand the mechanism of self-generated swirl in S-shaped diffusing ducts and the effect it has on the performance/flow characteristics of the duct. Rojas et al.[12] investigated the effect of developing laminar and turbulent flow on the characteristics of an S-shaped rectangular diffuser with moderate curvature. The pressure recovery achieved was approximately 20% of the velocity head. Seddon[13] explained the phenomenon of self-generated swirl and suggested means to overcome it. Some of the other important contributions are those of Shimzu et al.,[14,15] Whitelaw and Yu,[16] Lien and Leschzinger,[17] Majumdar et al.,[18] Gupta et al.,[19] and Anand et al.[20,21] The flow characteristics of S-shaped diffusing ducts are reasonably well understood but are not directly applicable to the divided intake ducts because of the basic difference in geometry and the complexity of the flow due to interaction of flow from the two limbs in the merging region. The complexity of the flow further increases when the flow rate in the two ducts is not the same and the velocity distribution is skewed at the inlet. In the present analysis, an attempt has been made to analyze the flow in a Y-shaped diffuser with each arm having a turn angle of 22.5/22.5 deg. The inlet of each arm is rectangular with an aspect ratio (AS) of 2.0 and the two arms join gradually into a circular outlet with area ratio of 2.0. Detailed flow analysis is carried out using the computational fluid dynamics (CFD) code FLUENT for uniform flow conditions at the inlet of both the ducts. Furthermore, analysis has been performed using unequal mass flow in the two limbs as well as skewed longitudinal velocity profiles in one of them. Computations are made for various velocity profiles having different skewness numbers and by keeping the average inlet velocity at 30, 60, and 90 m/s.

Received 20 August 2003; revision received 29 October 2003; accepted for publication 29 October 2003. Copyright © 2004 by the American Institute of Aeronautics and Astronautics, Inc. All rights reserved. Copies of this paper may be made for personal or internal use, on condition that the copier pay the $10.00 per-copy fee to the Copyright Clearance Center, Inc., 222 Rosewood Drive, Danvers, MA 01923; include the code 0021-8669/05 $10.00 in correspondence with the CCC.

*Research Associate, Department of Applied Mechanics.
†sidhnathsingh@hotmail.com.
‡Professor, Department of Applied Mechanics.

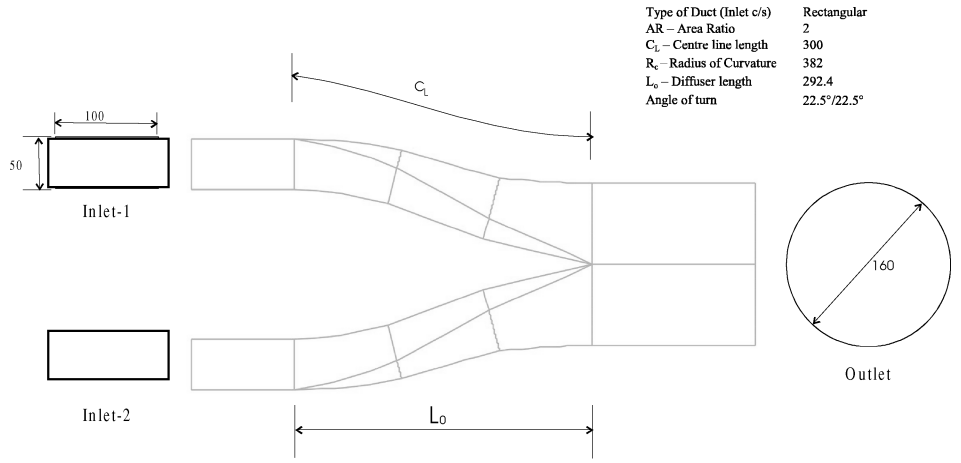

Fig. 1 Schematic diagram of divided intake ducts (rectangular crosssection).

Geometry of the Y-Shaped Duct

Figure 1 shows the schematic diagram of the Y-shaped diffuser. The dimensions of the rectangular duct at the inlet are 100×50 mm, where 100 mm is in the vertical direction. The outlet is circular with a diameter of 160 mm. The overall area ratio is 2.0. The required Y shape is generated by merging two similar S-shaped diffusers that have a rectangular inlet and semicircular outlet. Straight lengths of the ducts are added at both the inlets as well as at the outlet to facilitate the implementation of boundary conditions. Other geometrical details of the Y-shaped duct are given in the Fig. 1.

Mathematical Formulation

The governing equations in the reduced form for steady and incompressible flows are

$$\frac{\partial}{\partial x_i}(\rho u_i) = S_m \tag{1}$$

$$\rho u_j \frac{\partial u_i}{\partial x_j} = -\frac{\partial P}{\partial x_i} + \frac{\partial}{\partial x_j}\left[\mu\left(\frac{\partial u_i}{\partial x_j} + \frac{\partial u_j}{\partial x_i} - \frac{2}{3}\delta_{ij}\frac{\partial u_l}{\partial x_l}\right)\right] + \frac{\partial}{\partial x_j}(-\overline{\rho u_i' u_j'}) \tag{2}$$

where ρ is the density of the medium, u_i is the mean velocity in the ith directions, μ is the viscosity of the fluid, P is the static pressure, and u_i' are turbulent fluctuations.

The additional stress term in the momentum equation, $-\rho u_i' u_j$, is modeled using the standard k–ε turbulence model to obtain a closed set of equations. The choice of the standard k–ε turbulence model was made on the basis of the experience of Koutmos and McGuirk[22] and Majumdar.[23] They used this model for flow predictions in a dump diffuser and S-shaped diffuser, respectively, and found that it works reasonably well. In the k–ε two-equation model, the Boussinesq hypothesis is used to relate the Reynolds stresses to the mean velocity gradient:

$$-\overline{\rho u_i' u_j'} = \mu_t\left(\frac{\partial u_i}{\partial x_j} + \frac{\partial u_j}{\partial x_i}\right) - \frac{2}{3}\left(\rho k + \mu_t \frac{\partial u_i}{\partial x_i}\right)\delta_{ij} \tag{3}$$

where μ_t is the eddy viscosity, k is the turbulence kinetic energy, and δ_{ij} is the Kronecker delta function.

Two additional transport equations, one for turbulent kinetic energy (k) and the second for the turbulence dissipation rate (ε), are solved to evaluate μ_t, which is computed as follows:

$$\mu_t = \rho C_\mu k^2 \big/ \varepsilon \tag{4}$$

where C_μ is a constant.

The additional equations for k and ε for incompressible flow in simplified form in the absence of the thermal gradients are

$$\rho u_i \frac{\partial k}{\partial x_i} = \frac{\partial}{\partial x_i}\left[\left(\mu + \frac{\mu_t}{\sigma_k}\right)\frac{\partial k}{\partial x_i}\right] + G_k - \rho\varepsilon \tag{5}$$

$$\rho u_i \frac{\partial \varepsilon}{\partial x_i} + = \frac{\partial}{\partial x_i}\left[\left(\mu + \frac{\mu_t}{\sigma_\varepsilon}\right)\frac{\partial \varepsilon}{\partial x_i}\right] + C_{1\varepsilon}\frac{\varepsilon}{k}(G_k) - C_{2\varepsilon}\frac{\rho\varepsilon^2}{k} \tag{6}$$

where G_k is the generation of turbulent kinetic energy due to the mean velocity gradient, calculated as $G_k = \mu_t S^2$. In the following equation, S is the modulus of the mean rate of shear stress tensor, defined as

$$S = (2S_{ij}S_{ij})^{\frac{1}{2}} \tag{7}$$

and S_{ij} is given by

$$S_{ij} = \frac{1}{2}\left(\frac{\partial u_i}{\partial x_j} + \frac{\partial u_j}{\partial x_i}\right) \tag{8}$$

$C_{1\varepsilon}$ and $C_{2\varepsilon}$ are constants, and σ_k and σ_ε are the turbulent Prandtl numbers for k and ε, respectively. The values of constants in the turbulence model used in the present study are the standard values reported in the literature ($C_{2\varepsilon} = 1.92$, $C_{1\varepsilon} = 1.44$, $C\mu = 0.09$, $\sigma_k = 1.0$, and $\sigma_\varepsilon = 1.3$). These values have been found to work fairly well for a wide range of wall-bounded flows. The iterations were monitored by calculating the sum of absolute residuals for the mass, momentum, and so forth after each iteration and were normalized with the inlet values as follows:

$$\frac{\sum_{i=1}^{M} |R_i|^n}{S_{N\phi}} \leq 0.001 \tag{9}$$

where $|R_i|^n$ is the sum of absolute residuals for a dependent variable ϕ in the nth iteration and $S_{N\phi}$ is the corresponding normalizing factor. The iterations have been made using Cartesian coordinates while results are presented at different cross-sectional planes, making use of the built-in provision for postprocessing in the CFD package.

Data Analysis and Performance Parameter

The governing equations of motion have been solved using the CFD package to obtain the three-dimensional velocity field and pressure distribution at each point inside the flow domain. The

performances of the intake duct are quantitatively analyzed by calculating the following two coefficients.

The coefficient of pressure recovery (C_P) is defined as

$$C_P = \frac{\left(P_{S_o} - P_{S_i}\right)}{(P_{\text{dyn}})_{\text{in}}} \tag{10}$$

where P_{S_o} and P_{S_i} are the average values of the static pressure at the outlet and inlet, respectively, and $(P_{\text{dyn}})_{\text{in}}$ is the dynamic pressure corresponding to the average velocity at the inlet.

The coefficient of total pressure loss (C_L) is calculated as

$$C_P = \frac{\left(P_{t_o} - P_{t_i}\right)}{(P_{\text{dyn}})_{\text{in}}} \tag{11}$$

where P_{t_o} and P_{t_i} are the average total pressure at the outlet and inlet, respectively.

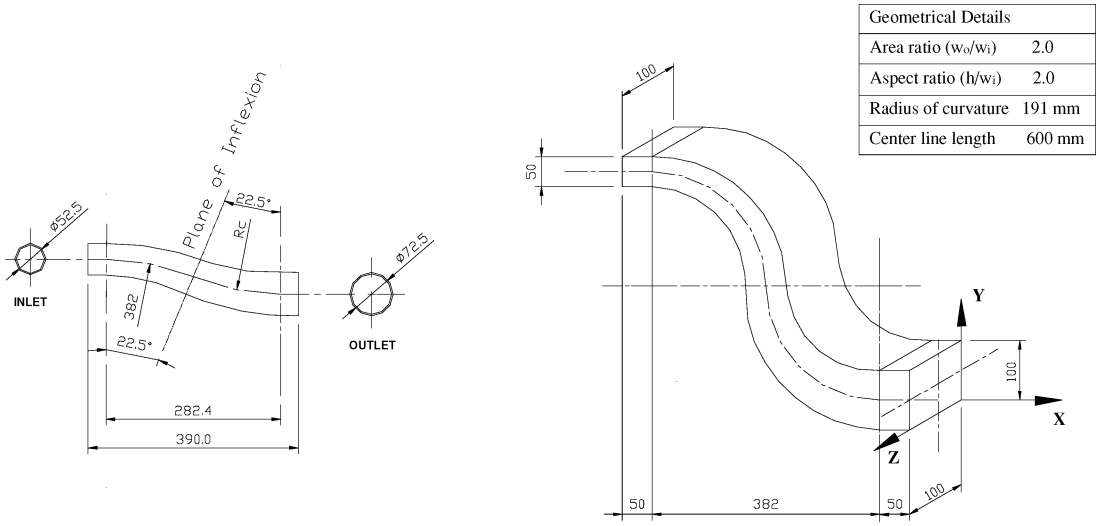

Fig. 2 Schematic layout of S-shaped rectangular and circular test diffusers used for code validation.

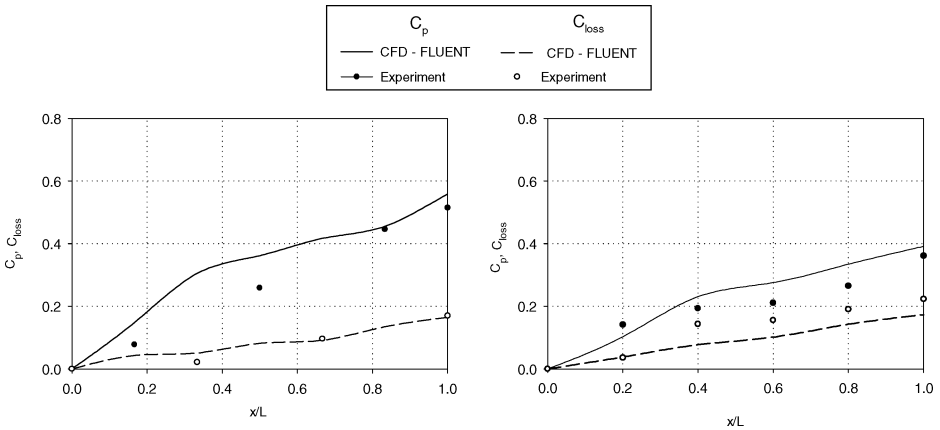

S-shaped rectangular diffuser (90/90 deg, 600 mm) **S-shaped circular diffuser 22.5/22.5 deg, 300 mm)**

Fig. 3a Comparison of performance parameters obtained through computational and experimental investigation.

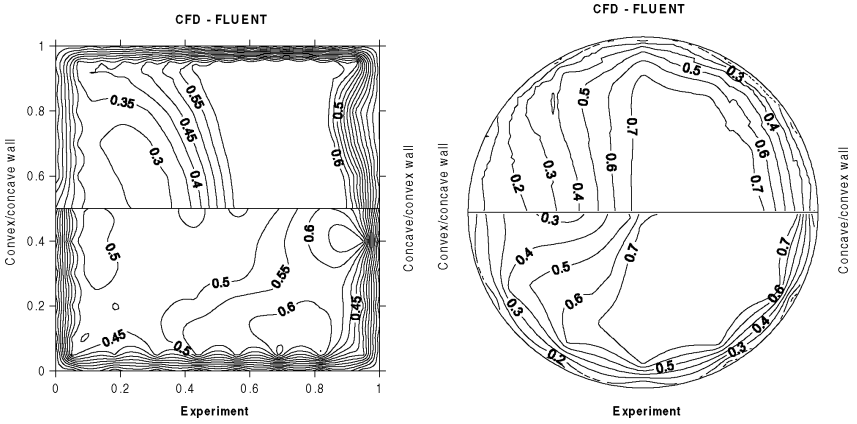

S-shaped rectangular diffuser (90/90 deg, 600 mm) **S-shaped circular diffuser (22.5/22.5 deg, 300 mm)**

Fig. 3b Comparison of normalized velocity distribution obtained through computational and experimental investigation.

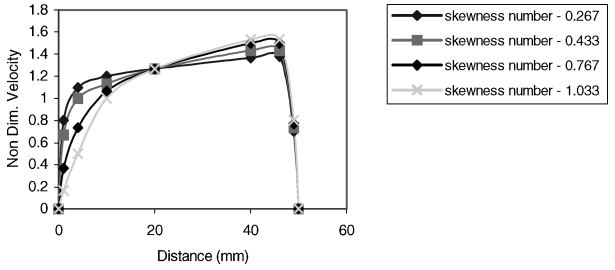

Fig. 4 Skewed inlet nondimensionalized velocity profile at duct 2.

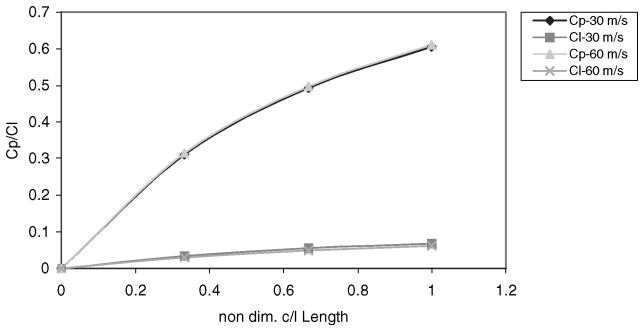

Fig. 5 Uniform inlet velocity at both inlets.

Validation of Code

The experimental results in a 90/90 deg S-shaped rectangular diffuser with an area ratio (AR) of 2 and AS = 2 carried out by Anand et al.[20] and in circular diffusers with AR = 1.9 by Anand et al.[21] are used for validating the code. The details of the geometries are given in Fig. 2. It is seen that the comparison is reasonably satisfactory for both geometries. Comparison between experimental and predicted performance parameters (C_p and C_L) is shown in Fig. 3a. There are minor deviations in the results, which could be attributed to higher wall roughness in the experiments. Predictions done with rough walls showed that a wall roughness of 0.5 mm showed improved matching with experimental results. The comparison of velocity distributions in the two geometries at the exit plane is presented in Fig. 3b. It is seen that the results match reasonably well. Minor deviations again can be attributed to the limitations of the turbulence model to handle zones of flow separation, wall curvature, and steep velocity gradients.

After validating the code, parametric investigation of Y-shaped divided intake ducts was carried out.

Discretization of the Flow Domain

The entire flow domain of the divided intake duct was modeled in GAMBIT and then the meshed geometry was exported to the FLUENT solver. Tetrahedral cells with a spacing of 7 mm were used for discretization and the total number of cells was 146471. Approximate time taken for computation was about 4 h on a Pentium IV processor for each set of runs.

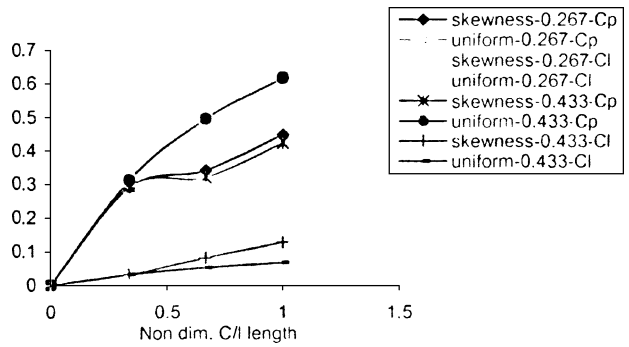

a) Skewness number: 0.267 and 0.433 (30 m/s)

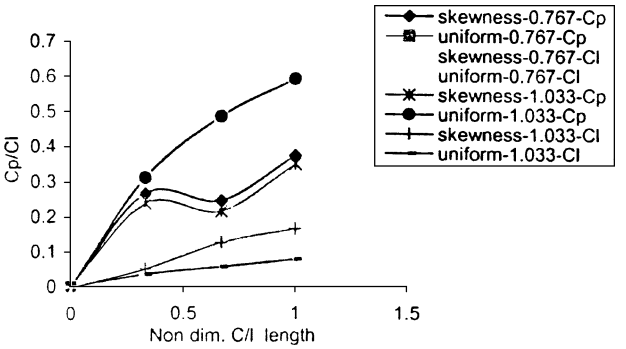

b) Skewness number: 0.767 and 1.033 (30 m/s)

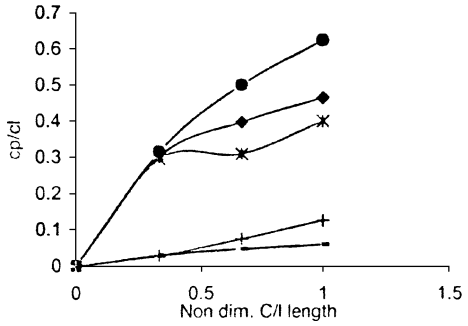

c) Skewness number: 0.267 and 0.433 (60 m/s)

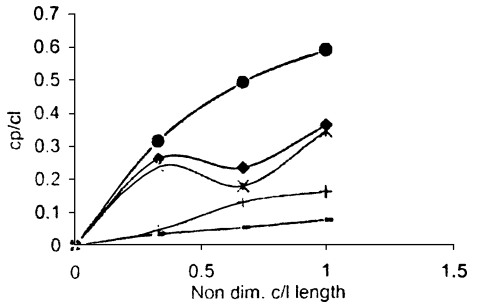

d) Skewness number: 0.767 and 1.033 (60 m/s)

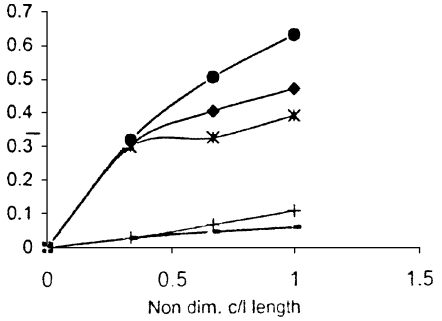

e) Skewness number: 0.267 and 0.433 (90 m/s)

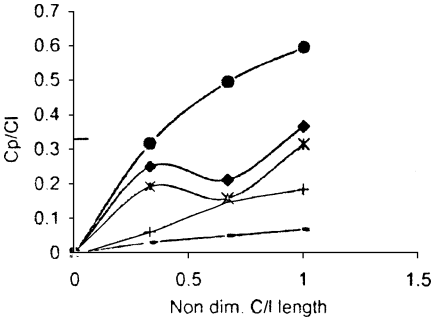

f) Skewness number: 0.767 and 1.033 (90 m/s)

Fig. 6 Variation of coefficients of static pressure recovery (C_P) and total pressure loss (C_L).

Results and Discussion

The various inlet conditions for the two limbs of the Y-shaped duct used to carry out the parametric investigations are given in Table 1. For the initial study, uniform flow is specified at the inlet for both limbs of the Y-shaped duct with average flow velocity of 30, 60, and 90 m/s. For other cases, the velocity profile at the inlet of one of the limbs is assumed to be uniform (inlet 1) with mass flow rate reducing with change in angle of attack, whereas skewed velocity profiles shown in Fig. 4 are specified at the inlet of the other limb (inlet 2) with mass flow remaining constant. The skewness number of the velocity profile is defined as the ratio of the difference in velocity at a distance of 5 and 45 mm from one of the sidewalls to the average velocity at that cross section. The range of skewness numbers covered is from 0.267 to 1.033 (see Fig. 4).

Table 1 Range of parameters investigated

Skewness number	Average skewed inlet velocity, Inlet 2, m/s	Average uniform inlet velocity, Inlet 1, m/s
0.267	30	28.5 (95%)
0.433	30	27 (90%)
0.767	30	24 (80%)
1.033	30	21 (70%)
0.267	60	57 (95%)
0.433	60	54 (90%)
0.767	60	48 (80%)
1.033	60	42 (70%)
0.267	90	85.5 (95%)
0.433	90	81 (90%)
0.767	90	72 (80%)
1.033	90	63 (70%)

The results obtained are presented in Figs. 5–12 in terms of C_p, C_L, longitudinal velocity distribution, and crossflow velocity distribution.

Figure 5 shows the variation of coefficients of static pressure and total pressure loss for uniform flow in both limbs with average inlet velocities of 30 and 60 m/s. It is observed that pressure recovery increases along the centerline length of the diffuser, but the rate of increase slows down after the point of inflection due to a change in the direction of the flow. The pressure recovery and pressure loss coefficients are almost the same for both average inlet velocities of 30 and 60 m/s. The maximum pressure recovery achieved for uniform inlet conditions is 0.62. The results for an inlet velocity of 90 m/s are similar. There are no significant effects of Reynolds number on the performance of the Y-shaped duct diffuser.

For skewed inlet velocity conditions at inlet 2 and uniform conditions at inlet 1, the variations of pressure coefficients are shown in Figs. 6a–6f. The variation of performance parameters has been shown separately for both limbs to facilitate the comparison. It is seen that the pattern of C_p and C_L for both inlets is quite different. In the limb in which inlet flow is uniform, the pressure recovery is nearly independent of Reynolds number even with the skewed velocity profile at the other inlet, because flow is always uniform throughout duct 1. The pressure recovery has a value of approximately 60%. The loss coefficient value is also nearly constant for this limb and is around 5%. For the limb with a skewed inlet velocity profile, the pressure linearly increases up to the inflection plane and then the rate of pressure recovery reduces gradually, whereas the loss coefficient increases linearly throughout the limb. The total pressure recovery in this limb is affected by both Reynolds number and skewness factor. The effect of Reynolds number is marginal, whereas with increasing skewness the pressure recovery reduces considerably. For a skewness factor of 0.267, the pressure

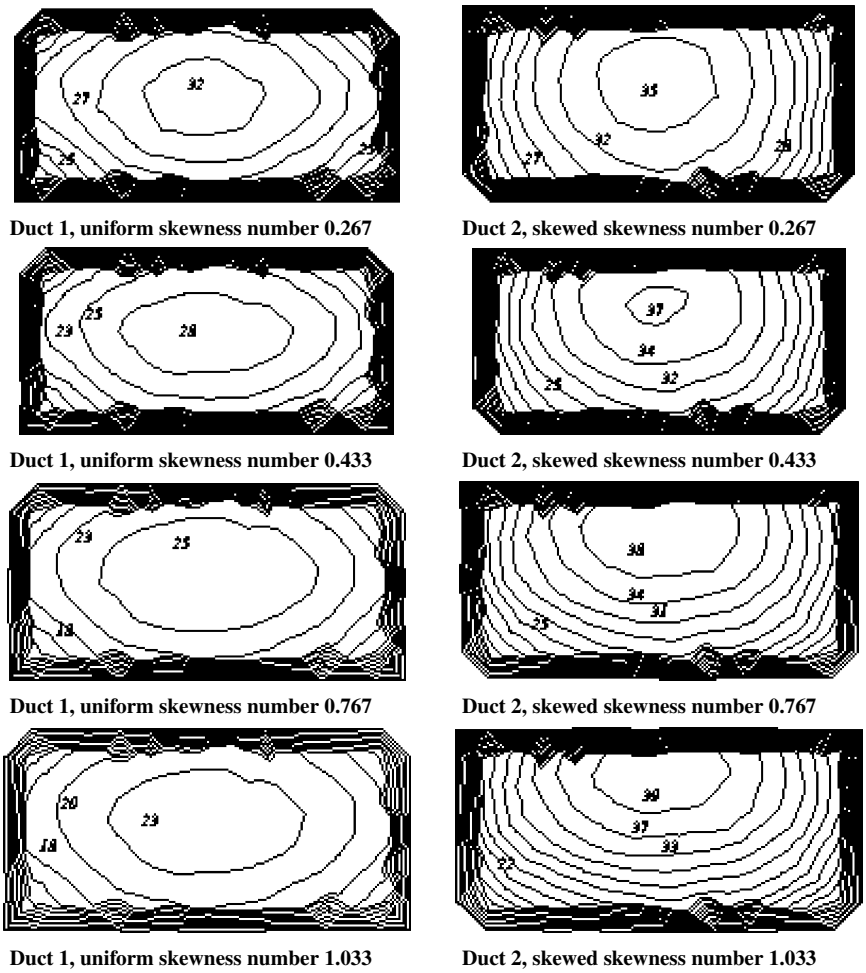

Fig. 7 Longitudinal velocity distribution at inlet for all conditions (angle of attack) 30 m/s.

Duct 1, 0 deg

Duct 2, 0 deg

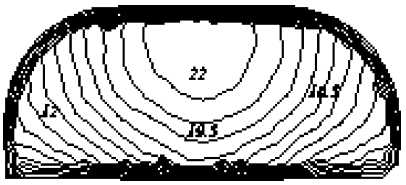

Duct 1, 22.5/7.5 deg

Duct 1, 22.5/7.5 deg

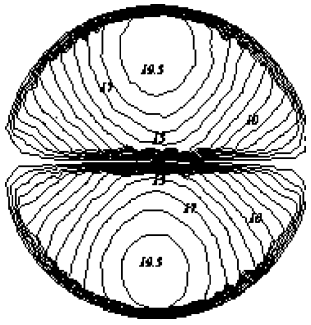

Merging plane, 22.5/22.5 deg

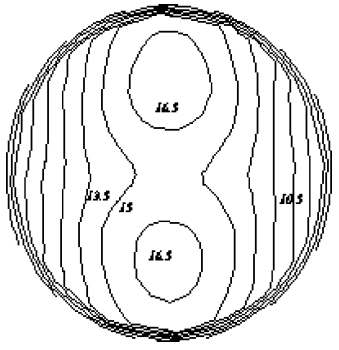

Outlet

Fig. 8 Longitudinal velocity distribution for uniform inlet velocity (30 m/s) at both ducts at different planes.

recovery is around 42%, whereas for a skewness factor of 1.033, the recovery is only 33%. The loss coefficient is also marginally affected by Reynolds number, whereas the effect of the skewness factor is quite pronounced. The value of C_L is around 10% for the lowest skewness and it increases to around 16% at the highest skewness.

Longitudinal Velocity

Longitudinal velocity contours in the two limbs for all inlet conditions are shown in Fig. 7. For the limb with uniform flows, a reduction in the peak velocity from 32 to 23 m/s is observed, whereas in the other limb the peak velocity is close to that for the fuselage side. The longitudinal velocity contours for uniform inlet conditions with average velocity at 30 m/s for both limbs are shown in Fig. 8.

It is observed that the magnitude of the contours decreases along the length of the limb due to diffusion. The contours corresponding to higher magnitude velocity remain near the outer side of the wall due to the curvature of the wall. At the outlet, the pattern of the contours is symmetrical and the order of magnitude of the higher velocities at the outlet is nearly 16.5 m/s. Core formation was observed at the outlet for all inlet conditions. The magnitude of the velocity contours increases with the increase in average inlet velocities. For the sake of brevity, the distributions for other inlet velocities are not presented here.

Longitudinal velocity contours at the merging plane and at the outlet for uniform flow in one limb and skewed in the other are presented in Figs. 9 and 10. The figures clearly indicate that the limb with skewed inlet velocity has a higher magnitude than that with the uniform inlet velocity. The higher velocity values remain near the outer side of the wall. The pattern of the velocity contours is not symmetrical at the outlet and the magnitude of the higher velocity contours ranges from 21 to 24 m/s. The magnitude of highest velocity increases with the increase in skewness factor of the velocity profile of the limb, whereas for uniform inlet profile the magnitude of the contours decreases with the increase in the angle of attack caused by the reduced mass flow conditions. Lower magnitude contours remain near the wall of the limb with uniform inlet conditions.

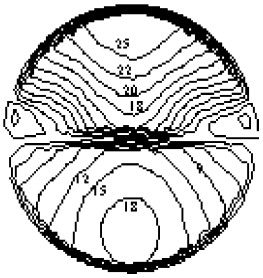

Skewed velocity at inlet 2 and uniform at inlet 1 (skewness number 0.267)

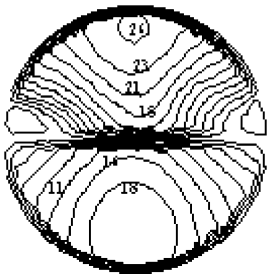

Skewed velocity at inlet 2 and uniform at inlet 1 (skewness number 0.433)

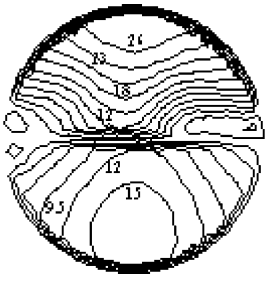

Skewed velocity at inlet 2 and uniform at inlet 1 (skewness number 0.767)

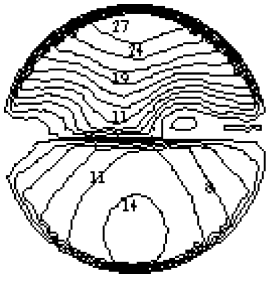

Skewed velocity at inlet 2 and uniform at inlet 1 (skewness number 1.033)

Fig. 9 Longitudinal velocity distribution at merging plane for different inlet conditions at a velocity of 30 m/s.

The formation of the core was also observed at the outlet near the wall of the limb with skewed inlet conditions.

Crossflow Velocity Vectors

Crossflow velocity vector distribution is shown in Figs. 11 and 12. It is observed that strong cross-velocity components are present throughout the length of the limbs for all inlet conditions. The magnitude of the velocity vectors decreases along the length of

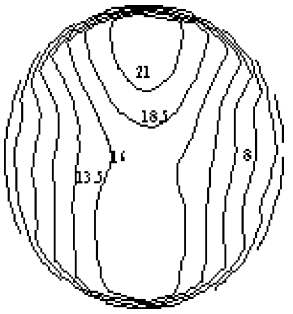

Skewed velocity at inlet 2 and uniform at inlet 1 (skewness number 0.267)

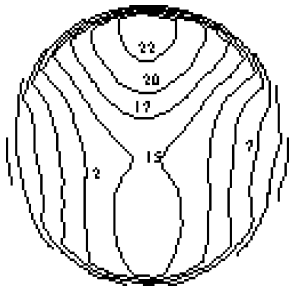

Skewed velocity at inlet 2 and uniform at inlet 1 (skewness number 0.433)

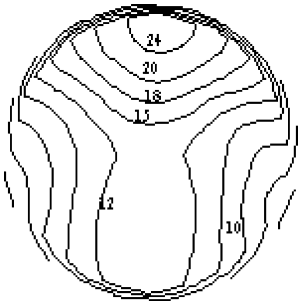

Skewed velocity at inlet 2 and uniform at inlet 1 (skewness number 0.767)

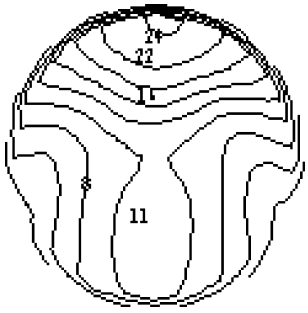

Skewed velocity at inlet 2 and uniform at inlet 1 (skewness number 1.033)

Fig. 10 Longitudinal velocity distribution at the exit for various inlet conditions at a velocity of 30 m/s.

Duct 1 inlet

Duct 2 inlet

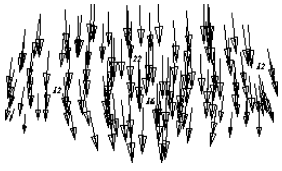

Duct 1, 22.5/7.5 deg

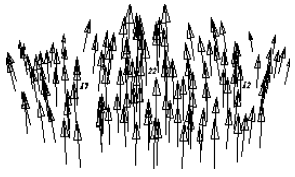

Duct 2, 22.5/7.5 deg

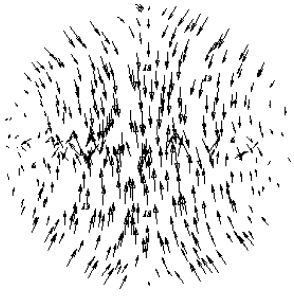

Merging Plane, 22.5/22.5 deg

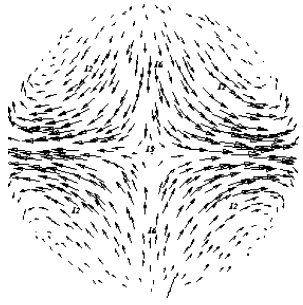

Outlet

Fig. 11 Cross velocity vector distribution for uniform inlet velocity at both limbs.

the diffuser. It is also observed that two pairs of counter-rotating vortices are formed at the outlet for uniform inlet conditions in both limbs (Fig. 11), whereas in the case where one limb has a skewed inlet velocity profile the pattern is quite different (Fig. 12). Two pairs of counter-rotating vortices are observed for skewness numbers of 0.267 and 0.433. The magnitude of the vectors is greater in the limb with skewed inlet conditions. The pattern is also not symmetrical in these cases. For higher skewness number, one pair of counter-

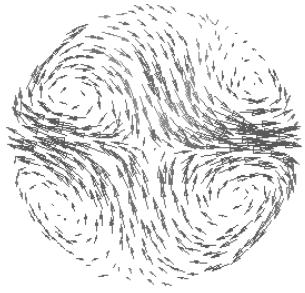

Skewed velocity at inlet 1 and uniform at inlet 2 (skewness number 0.433)

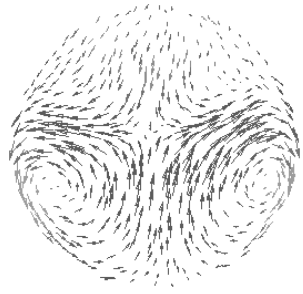

Skewed velocity at inlet 1 and uniform at inlet 2 (skewness number 0.267)

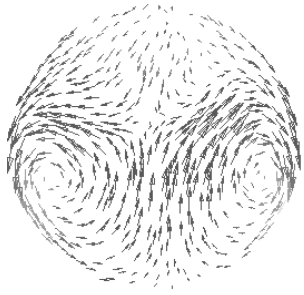

Skewed velocity at inlet 1 and uniform at inlet 2 (skewness number 1.033)

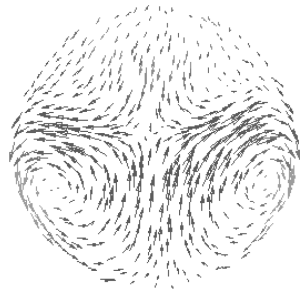

Skewed velocity at inlet 1 and uniform at inlet 2 (skewness number 0.767)

Fig. 12 Crossflow velocity vector distribution at the exit for various inlet conditions at a velocity of 30 m/s.

rotating vortices becomes very strong and is present in the limb with uniform inlet conditions. The second pair of counter-rotating vortices is very weak and is difficult to identify. The highest magnitude of the crossflow velocity vectors is found to be in the range of 10 to 23 m/s at the outlet for all skewness conditions. The crossflow velocity vector distribution for 60 and 90 m/s was also observed to be nearly same and is not shown here for the sake of brevity.

Conclusions

After investigating the flow behavior of divided intake Y-shaped diffuser for different velocity profiles at the two inlets, the following conclusions can be drawn:

The coefficient of static pressure recovery and total pressure loss are not significantly affected by the increase in Reynolds number.

No separation is observed along the length of the diffuser.

The performance of the Y-shaped diffusing duct deteriorates with the increase in skewness of the inlet velocity profile.

Two pairs of counter-rotating vortices of equal intensity are observed at the exit for skewness factors of 0.267 and 0.433, whereas one strong pair and one weak pair of vortices are found at higher skewness factors.

The flow is more complex in inlet duct 2 (skewed inlet velocity profile) compared to the other inlet duct.

The flow behavior in the Y-shaped duct becomes more and more disturbed as the skewness is increased.

References

[1]Martin, N. J., and Holzhauser, C. A., "Analysis of Factors Influencing the Stability Characteristics of Symmetrical Twin-Intake Air-Induction Systems," NACA TN 2049, March 1950.

[2]Simon, P. C., "Performance Characteristics at Mach Numbers to 2.0 of Various Types of Side Inlets Mounted on Fuselage of Proposed Supersonic Airplane IV-Rectangular-Cowl Inlets with Two-Dimensional Compression Ramps," NACA RM E52H29, Oct. 1952, p. 39.

[3]Obery, L. J., and Stitt, L. E., "Investigations at Mach Numbers 1.5 and 1.7 of Twin-Duct Side Air-Intake System with 9° Compression Ramp Including Modifications to Boundary Layer Removal Wedges and Effects of a Bypass System," NACA RM E53H04, Oct. 1953.

[4]Pai, T. G., "Aerodynamic Testing of Air Intake for a Modern Combat Aircraft," *Discussion Meeting on Aerodynamic Testing and Structural Dynamics*, Interline Publishing, Bangalore, India, 1994, pp. 93–110.

[5]Sudhakar, K., and Ananthkrishnan, N., "Jump Phenomena in Y-Shaped Intake Ducts," *Journal of Aircraft*, Vol. 33, No. 2, 1995, pp. 438, 439.

[6]Jolly, R., Pai, T. G., and Jayasimha, P., *Design and Development of a Bifurcated Y-Duct Intake for a Modern Combat Aircraft*, *Journal of the Aeronautical Society of India*, Vol. 54, No. 2, 2002, pp. 125–131.

[7]Bharani, S., Singh, S. N., Seshadri, V., and Chandramoulli, R., "Performance Evaluation of Divided Intake Ducts: Effects of Area Ratio and Inlet Reynolds Number," *Fluid Dynamics Research*, International Journal of Fluid Mechanics Research, 2004 (to be published).

[8]Bharani, S., Singh, S. N., Seshadri, V., and Chandramoulli, R., "Effect of Angle of Turn on Performance of Divided Intake Ducts," *Proceedings of the Institute of Mechanical Engineers, Part G: Journal of Aerospace Engineering*, Vol. 218, 2004 (to be published).

[9]Guo, R. W., and Seddon, J., "An Investigation of the Swirl in an S-Duct," *Aeronautical Quarterly*, Vol. 33, Feb. 1982, pp. 25–58.

[10]Guo, R. W., and Seddon, J., "Swirl Characteristics of an S-Shaped Air Intake with Horizontal and Vertical Offsets," *Aeronautical Quarterly*, Vol. 34, May 1983, pp. 130–146.

[11]Guo, R. W., and Seddon, J., "The Swirl in an S-Duct of Typical Air Intake Proportions," *Aeronautical Quarterly*, Vol. 34, May 1983, pp. 99–129.

[12]Rojas, J., Whitelaw, J. H., and Ylanneskis, M., "Developing Flow in S-Shaped diffusers," Rept. FS/83/21, Imperial College of Science and Technology, Dept. of Mechanical Engineering, 1983.

[13]Seddon, J., "Understanding and Countering the Swirl in S-ducts: Tests on the Sensitivity of Swirl Fences," *Aeronautical Journal*, 1984, pp. 117–127.

[14]Shimizu, Y., Futaki, Y., and Martin, C. S., "Secondary Flows and Hydraulic Losses Within Sinuous Consists of Rectangular Cross-Section," *Journal of Fluids Engineering*, Vol. 114, Dec. 1992, pp. 593–609.

[15]Shimizu, Y., Nagfusa, M., Sugino, K., and Nakamura, S., "Studies on Performance and Internal Flow of Twisted S-Shaped Bend Diffuser: 1st Report," *Journal of Fluids Engineering*, Vol. 108, Sept. 1986, pp. 286–296.

[16]Whitelaw, J. H., and Yu, S. C. M., "Turbulent Flow Characteristics of S-Shaped Diffusing Ducts," *Flow Measurement and Instrumentation*, Vol. 4, No. 3, 1993, pp. 171–179.

[17]Lien, F. S., and Leschzinger, M. A., "Computational Modeling of 3-D Turbulent Flow in S-Diffuser and Transition Ducts," *Engineering Turbulence Modeling and Experiments*, edited by W. Rodi, and F. Martelli, Elsevier Science Publ., Florence, Italy, 1993.

[18]Majumdar, B., Singh, S. N., and Agarwal, D. P., "Flow Characteristics in S-Shaped Diffusing Duct," *International Journal of Turbo and Jet-Engines*, Vol. 14, No. 1, 1997, pp. 45–57.

[19]Gupta, V., Devpura, R., Singh, S. N., and Seshadri, V., "Effect of Aspect Ratio and Curvature on Characteristics of S-Shaped Diffusers," *Indian Journal of Engineering and Materials Sciences*, Vol. 8, June 2001, pp. 141–148.

[20]Anand, R. B., Lajpat, R., Singh, S. N., and Sharma, O. P., "Flow Characteristics of a Low Aspect Ratio 90°/90° S-Shaped Diffuser," *Journal of the Aeronautical Society of India*, Vol. 53, No. 4, 2001, pp. 239–252.

[21]Anand, R. B., Lajpat, R., and Singh, S. N., "Flow and Performance Characteristics of a 22.5°/22.5° S-Shaped Circular Diffuser," *Proceedings of the 28th National Conference on FMFP*, Punjab Engineering College, Chandigarh, India, 13–15 Dec. 2001.

[22]Koutmos, P., and Mc Guirk, J. J., "Numerical Calculations of the Flow in Annular Combustor Dump Diffuser Geometries," *Proceedings of the Institution of Mechanical Engineers*; also *Part C Journal of Mechanical Engineering Science*, Vol. 203, 1998.

[23]Majumadar, B., "Flow Characteristics of Curved Diffusers," Ph.D. Dissertation, Dept. of Applied Mechanics, Indian Institute of Technology, New Delhi, India, 1994.